J. Plasma Physics (2000), *vol.* 64, *part* 1, *pp.* 75–87. Printed in the United Kingdom

Ion-beam–plasma electromagnetic instabilities

K. GOMBEROFF[1], L. GOMBEROFF[2] and H. F. ASTUDILLO[3]

[1] RAFAEL, Haifa, PO Box 2250, Israel 31021
[2] Departamento de Física, Facultad de Ciencias, Universidad de Chile, Casilla 653, Santiago, Chile
[3] Departamento de Física, Universidad de Concepción, Casilla 4009, Concepción, Chile

(Received 3 August 1999 and in revised form 31 August 1999)

Abstract. It is well known that ion-beam–plasma interactions can destabilize right- and left-hand polarized electromagnetic waves. Owing to the fact that these instabilities have mostly been studied numerically by solving the hot-plasma dispersion relation, their fluid nature has often gone unnoticed. Choosing the ion background to be the rest frame, it is shown that the right-hand polarized instabilities are the result of a merging of the magnetosonic/electron-cyclotron branch of the dispersion relation with the ion beam. For any given ion-beam density and sufficiently large beam velocity, there are always two right- and two left-hand polarized instabilities leading to forward-propagating electromagnetic waves. It is also shown that all right-hand polarized instabilities are resonant instabilities, satisfying $\omega - kU + \Omega_p \approx 0$ around their maximum growth rate (ω and k are the frequency and the wavenumber respectively, U is the beam velocity, and Ω_p is the proton gyrofrequency). Likewise, when the two left-hand instabilities are simultaneously present, they are also resonant instabilities satisfying $\omega \approx \Omega_p$. The high-frequency right-hand resonant instability ($\omega \gg \Omega_p$) has a maximum growth rate that depends only on the ratio between the beam density and the total density. The range of the unstable spectrum decreases with increasing beam velocity, leading to highly monochromatic radiation.

1. Introduction

Electromagnetic ion-beam–plasma instabilities have been thoroughly investigated over the years, both in the linear (see e.g. Gary 1991) and in the nonlinear theory (see e.g. Hollweg et al. 1993; Gomberoff et al. 1994).

Field-aligned ion beams have been detected in the solar wind (Feldman et al. 1974), in the plasma-sheet boundary layer (DeCoster and Frank 1970; Forbes et al. 1981; Eastman et al. 1984; Takahashi and Hones 1988), and in cometary exospheres (Coates et al. 1989; Neugebauer et al. 1989). However, the most outstanding examples of various ion beams generating many forms of electromagnetic fluctuations can be found in the region upstream the terrestrial foreshock (Hoppe et al. 1981, 1982).

Most of the work is related to low-frequency waves ($\omega \leqslant \Omega_p$). However, Goldstein and Wong (1987) (see also Wu and Davidson 1972), studying low-frequency waves observed at comet Giacobini–Zinner (Tsurutani and Smith 1986), showed that the newborn pickup ion-beam distribution function (in the solar-wind frame), can also destabilize high-frequency modes, which they called

'high-frequency whistler-like modes'. These whistler-like modes have also been studied in connection with the Earth's foreshock (Akimoto et al. 1987, 1993; Wong and Goldstein 1987; Akimoto and Winske 1989). These modes have frequencies well above the ion-beam gyrofrequency. Later, Brinca and Tsurutani (1988a,b), in a survey of low-frequency electromagnetic waves stimulated by two coexisting newborn ion species, showed that ion beams can indeed generate these high-frequency right-hand waves. They also showed that high-frequency left-hand waves ($\omega > \Omega_i$), are also unstable, but here the free-energy source of the instability is the thermal anisotropy of the ion-beam distribution function.

It has recently been shown that in the cold-plasma theory, the ion beam destabilizes left- and right-hand polarized waves in such a way that, depending on the ion-beam velocity and concentration, the unstable spectrum may have a band structure for right- and left-hand modes (Gnavi et al. 1996; Gomberoff et al. 1996). It was also shown that for low thermal energies, the band structure persists and, as the temperatures of the beam and the background increase, the band structure becomes a double-humped spectrum (Gomberoff and Astudillo 1998).

A double-humped structure for left-hand polarized waves has also been discussed by Brinca et al. (1990), in connection with ion-beam–plasma interactions. However, these structures are due to thermal anisotropies of the core and/or the ion beam, and have nothing to do with the band structure studied by Gomberoff and Astudillo (1989).

As pointed out above, in the presence of thermal effects and for right-hand polarized costreaming ion beams, the band structure was noticed by Brinca and Tsurutani (1988a). They also noticed that some of the instabilities found by them may have a purely fluid-like behaviour.

We show here that of all the mentioned ion-beam–plasma electromagnetic instabilities are in fact fluid instabilities. The right-hand polarized instabilities are due to the merging of the magnetosonic/electron-cyclotron branch of the dispersion relation with the ion beam. For large beam velocities, the unstable range become very narrow, leading to nearly monochromatic radiation. Thermal effects on the core ion lead to a decrease in the growth rate of the low-frequency branch of the spectrum, but does not change the instability range. On the other hand, thermal effects on the ion beam lead to a decrease in the growth rate of the high-frequency branch of the spectrum and also to a broadening of the instability range. As noticed in Akimoto et al. (1987), Wong and Goldstein (1988), and Akimoto and Winske (1989), a beam thermal anisotropy larger than 1, $T_\perp/T_\parallel > 1$, leads to an increase in the growth rate of the high-frequency branch of the unstable spectrum, and also to an enhancement of the instability range.

The paper is organized as follows. In Sec. 2, we show that all the aforementioned ion-beam–plasma electromagnetic instabilities are present in a purely cold-plasma theory. Some analytical results concerning growth rates and instability widths are derived. In Sec. 3, we solve the hot-plasma dispersion relation numerically in order to show that 'thermal effects lead in general to a decrease of the cold-plasma instabilities and to an increase in the width of the unstable spectrum. The only exception is the electron/ion whistler instability, which for thermal anisotropies satisying $T_\perp > T_\parallel$ can lead to a substantial

increase in the growth rate of the unstable spectrum. In Sec. 4 we summarize and discuss the results.

2. The dispersion relation

We shall assume a background plasma composed of electrons and protons, and an electron and a proton beam moving in the direction of an external magnetic field. The rest frame is chosen to be the background protons. For the proton background, we shall assume a Maxwellian distribution function, and a drifting Maxwellian for the proton beam. Assuming the plasma to be locally uniform, the dispersion relation for left-hand waves is given by

$$y^2 = A_c - 1 - x - \frac{1}{y\beta_{\|p}^{1/2}} Z\left(\frac{x-1}{y\beta_{\|p}^{1/2}}\right)[(A_c-1)(1-x)-x] + \eta(A_b-1)$$
$$-\eta(x-yU) - \frac{\eta}{y\beta_{\|b}^{1/2}} Z\left(\frac{(x-yU)-1}{y\beta_{\|b}^{1/2}}\right)[(A_b-1)(1-x+yU)$$
$$-(x-yU)], \tag{1}$$

where $y = kV_A/\Omega_p$, $x = \omega/\Omega_p$, $V_A = B_0/(4\pi n_p m_p)^{1/2}$ is the Alfvén velocity, $\eta = n_b/n_c$, $\beta_{\|i} = 8\pi n_i K T_{\|i}/B_0^2$ (where K is Boltzmann's constant), Z is the plasma dispersion function (Fried and Conte 1961), $U = V_b/V_A$ (where V_b is the beam velocity), and $A_l = T_{\perp l}/T_{\|l}$ is the thermal anisotropy and $T_\|$ ($T_\perp$) refers to the temperature parallel (perpendicular) to the external magnetic field, and the index l refers to the proton core and the proton beam. In deriving (1), we have assumed the plasma to be current-free, $\Sigma_l q_l n_l V_l = 0$, where l stands for the electron background, proton background (p), electron beam, and proton beam (b) (see e.g. Gomberoff 1992, 1995). The electrons, although not cold, can be assumed to be so because the argument of the plasma dispersion function is much larger than 1 in the frequency region of interest ($\omega \ll \Omega_p$). Note also that we have chosen the rest frame to be the proton background.

On taking the cold-plasma limit, the dispersion relation reduces to

$$y^2 = \frac{x^2}{1-x} + \frac{\eta(x-yU)^2}{1-(x-yU)}. \tag{2}$$

The instability thresholds can be determined following the procedure of Gnavi et al. (1996) (see also Gomberoff and Astudillo 1998). Thus, in Fig. 1 we have plotted y versus U for several values of η. The upper half-plane corresponds to left-hand waves and the lower half-plane to right-polarized waves. In this figure, the curves correspond to isodensity contours for various η values as functions of y and U. The instability regions in y space for a given beam velocity and density depend on the U value. For example, for $U = 3$, there are two unstable regions – one corresponding to left-hand waves ranging from $y \approx 0.1$ to $y = 0$, and the other to right-hand waves ranging from $y \approx -2.4$ to $y = 0$. On the other hand, when the vertical line crosses two or three isodensity contours corresponding to the same η value, the instability regions correspond to the chords between the isodensity curves. For example, for $U = 4$ and $\eta = 0.4$, the corresponding vertical line crosses two isodensity curves, leading to one unstable region for left-hand waves, between $y = 0$ and $y \approx 1.25$, and two for

https://doi.org/10.1017/S0022377800008436 Published online by Cambridge University Press

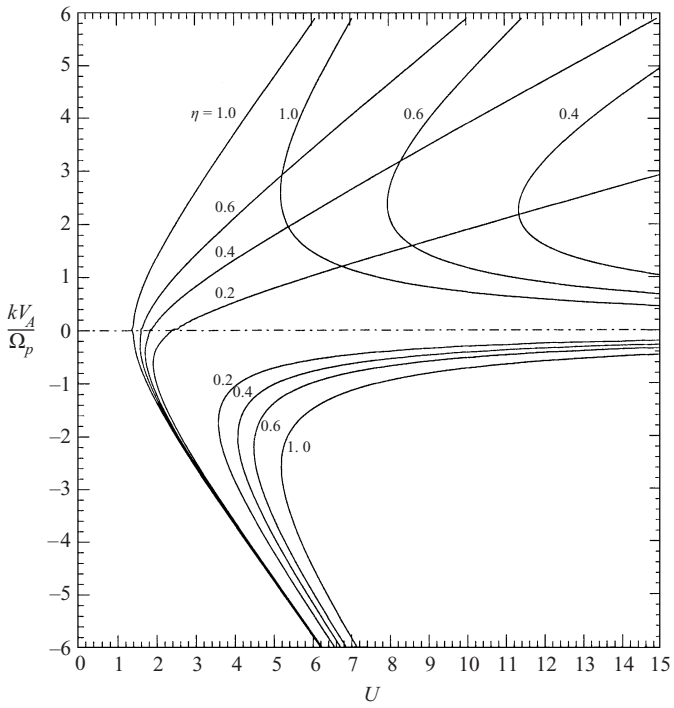

Figure 1. Instability thresholds, $y = kV_A/\Omega_p$ versus $U = V_b/V_A$, for several values of $\eta = n_b/n_e$. The upper half-plane refers to right-hand waves, and the lower one to left-hand waves.

right-hand waves, one ranging from $y = 0$ to $y \approx -1$, and the other from $y \approx -2.4$ to $y \approx -3.8$. When there are three isodensity curves involved, there are two unstable regions for each polarization.

Thus it follows from Fig. 1 that for $\eta \leqslant 1$, the system becomes unstable when $U \geqslant 1.4$. It also follows that for any $\eta \leqslant 1$, there is a threshold value of U, $U_t(\eta)$, in the internal $1.4 \leqslant U_b \leqslant 5.1$ such that for $U > U_t$, there are two instability regions for right-hand waves. In this interval, there is only one instability for left-hand waves. As follows from Fig. 1, when $\eta = 1$ and $U \approx 5.1$, there are two instability regions for left-hand waves as well. For other values of η, there are also two instability regions for left-hand waves, provided that $U > U_t(\eta) > 5.1$. It follows from Fig. 1 that for decreasing values of η, larger and larger values of U are required to destabilize the high-wavenumber branch of left-hand waves.

In order to illustrate the various possibilities just described, we have plotted in Fig. 2 the dispersion relation, y versus x, for $\eta = 0.2$ and several values of U. The first quadrant corresponds to left-hand waves propagating in the direction of the external magnetic field. In the second quadrant, we have enlarged the first quadrant. The third quadrant corresponds to right-hand waves propagating forward, and the fourth quadrant is for right-hand waves propagating backwards. Thus in Fig. 2(a), we have taken $\eta = 0.2$ and $U = 1.5$ in order to illustrate the dispersion branches when the system is stable. In Fig. 2(b), we have increased U to $U = 2$. As follows from Fig. 1, there is only one instability region corresponding to right-hand waves. In Fig. 2(c), we have increased U to $U = 3$. There are two unstable regons, one for each polarization. Next, in Fig.

https://doi.org/10.1017/S0022377800008436 Published online by Cambridge University Press

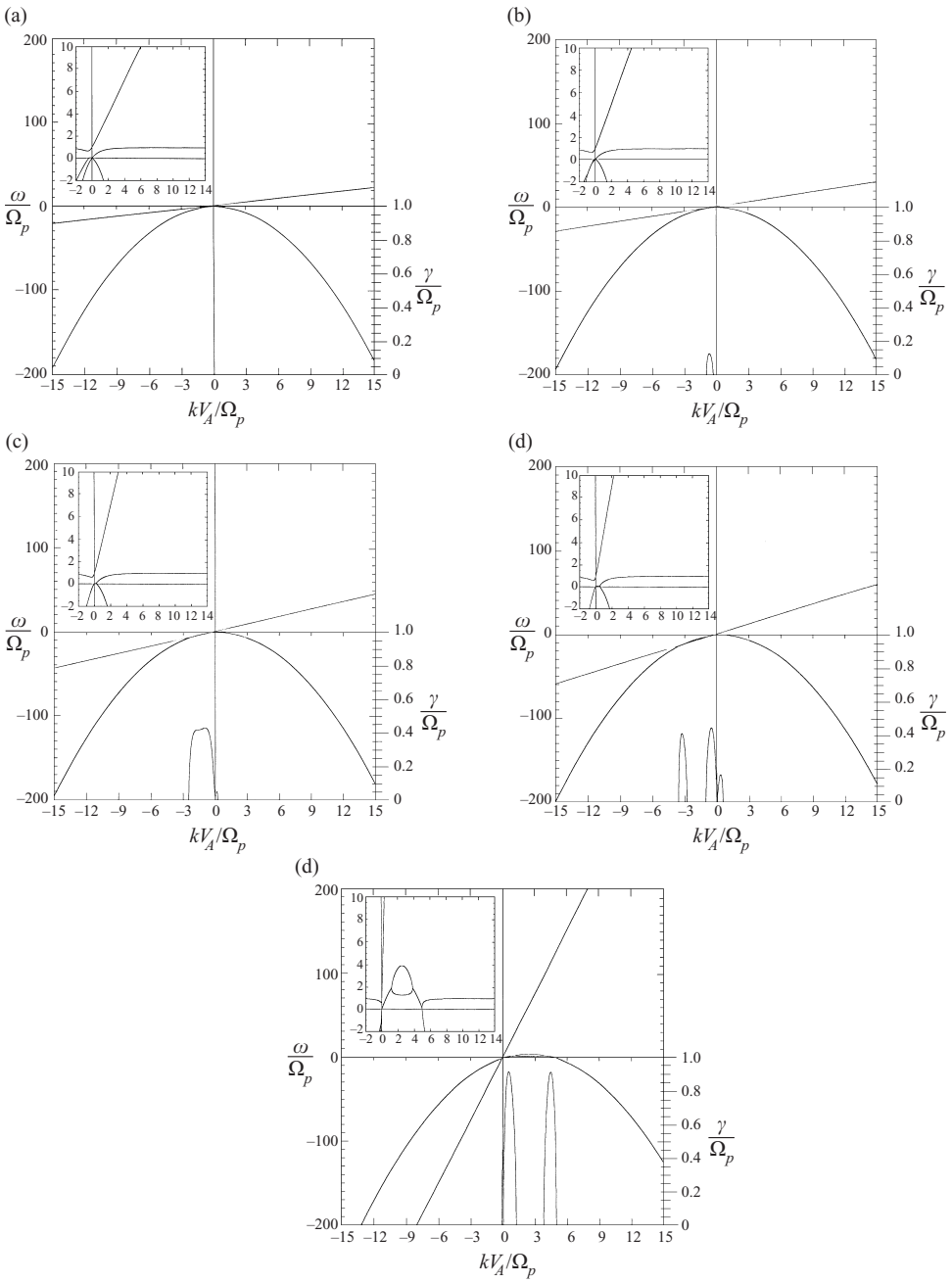

Figure 2. (a) Cold-plasma dispersion relation, $x = \omega/\Omega_p$ versus y, for $\eta = 0.2$ and $U = 1.5$. The first quadrant corresponds to left-hand waves and the third to right-hand waves. The figure in the second quadrant is an enlargement of the first quadrant. (b) $U = 2$. The two curves around the origin are the normalized growth rates, γ/Ω_p. (c) $U = 3$. (d) $U = 4$. (e) $U = 25$.

https://doi.org/10.1017/S0022377800008436 Published online by Cambridge University Press

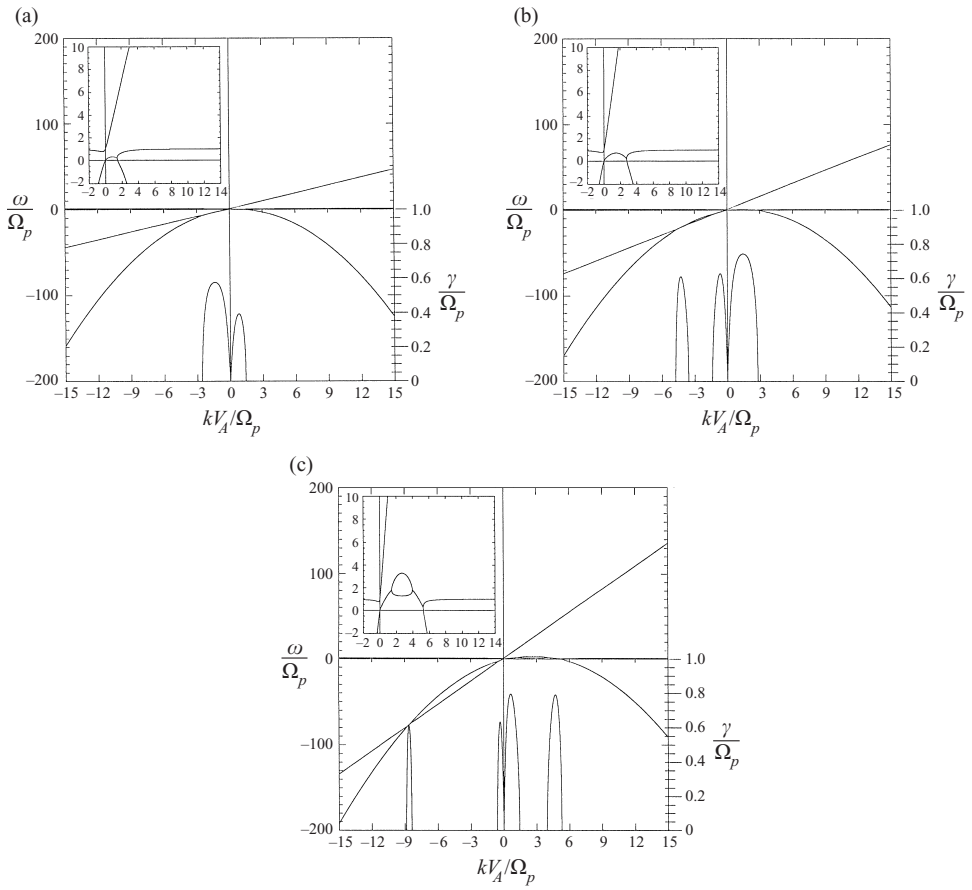

Figure 3. (a) As Fig. 2, but for $\eta = 0.6$ and $U = 3$. (b) $U = 5$. (c) $U = 9$.

2(d), we have increased U to $U = 4$. Note that in this case, $U_t \approx 3.8$. There are two unstable regions for right-hand waves and one for left-hand waves. Finally, in Fig. 2(e), we have increased $U_b = 25$ in order to show that there are four unstable regions, two for each polarization. The high-frequency right-hand instability is not shown in the figure. It occurs for $x \approx 630$ and $y \approx 25$, in a region where ω cannot be neglected relative to Ω_e (the electron gyrofrequency), and therefore the dispersion relation is no longer valid. Note that the right-hand instability is due to the merging of the electron–magnetosonic branch of the dispersion relation with the ion-beam branch. The ion-beam branch is a straight line satisfying $x - yU = \pm 1$. The plus (minus) sign refers to left (right) polarization.

In Fig. 3, we have done the same as in Fig. 2, but not for $\eta = 0.6$. Thus, in Fig. 3(a), we have set $U = 3$. We see that there are two instability regions (note the small peck in the fourth quadrant), one for each polarization, as in Fig. 2(c). In Fig. 3(b), we have increased U to $U = 5$ in order to show that there are two instability regions corresponding to right-hand waves and one corresponding to left-hand waves, as in Fig. 2(d). In Fig. 3(c), we have increased U to $U = 9$. There are now four instability regions, two for each polarization.

In order to determine the growth rates, in (2), we replace x by $x + i\gamma/\Omega_p$,

https://doi.org/10.1017/S0022377800008436 Published online by Cambridge University Press

where x is real. In order to make the denominators on the right-hand side of (2) real quantities, we multiply and divide each fraction by the complex conjugate of the corresponding denominator. Equating the imaginary part to zero yields the following equation for the normalized growth rate $\Gamma = \gamma/\Omega_p$:

$$\Gamma^4 + [(1 \pm x)^2 + (1 \pm x \mp U_y)^2 - 1]\,\Gamma^2$$

$$+ (1 \pm x)^2(1 \pm x \mp yU)^2 - \frac{(1 \pm x \mp yU)^2 + \eta(1 \pm x)^2}{1+\eta} = 0, \tag{3}$$

where the upper (lower) sign refers to right-hand (left-hand) polarized waves. Thus the sign of x and y for right- and left-hand waves is now always positive.

Let us concentrate first on the right-hand instabilities. As pointed out above, for a given ion-beam density and sufficiently large beam velocities, there are always two instability regions. The high-frequency instability region occurs for $\omega \gg \Omega_p$. Thus, assuming $x \gg 1$, $x \gg |1 + x - yU|$, and $\Gamma \ll x$, (3) can be approximated by

$$x^2\Gamma^2 + x^2(1 + x - yU)^2 - \frac{x^2\eta}{1+\eta} \approx 0, \tag{4}$$

so that

$$\Gamma^2 \approx \frac{\eta}{1+\eta} - (x - yU + 1)^2. \tag{5}$$

It follows from this expression that the maximum growth rate occurs for $x - yU + 1 \approx 0$, and is given by

$$\Gamma_{\max} \approx \sqrt{\frac{\eta}{1+\eta}}. \tag{6}$$

Thus the maximum growth depends only on η. We see from Fig. 2(d) that the maximum growth of the right-hand high-frequency branch of the instability occurs for $\Gamma \approx 0.4$. On the other hand, it follows from Fig. 3(c) that $\Gamma \approx 0.61$. These values are in very good agreement with (5).

On the other hand, it follows from the real part of (2) that for $x \gg 1$ and $x \gg \Gamma$,

$$y^2 \approx x + \frac{\eta(x - yU)^2(1 + x - yU)}{(1 + x - yU)^2 + \Gamma^2} + \frac{\eta\Gamma^2(x - yU - 1)}{(1 + x - yU)^2 + \Gamma^2}. \tag{7}$$

Using (5), the denominators in (7) can be replaced by $\eta/(1+\eta)$. Thus (6) can be written in the form

$$y^2 \approx x + (1+\eta)\,(x - yU)^2(1 + x - yU) + (1+\eta)\,\Gamma^2(x - yU - 1). \tag{8}$$

In order to calculate the instability range, we use the fact that the marginal modes satisfy $\Gamma = 0$:

$$1 + x - yU \approx \pm\sqrt{\frac{\eta}{1+\eta}}. \tag{9}$$

Upon replacing (8) into (7), we obtain for the marginal modes

$$y_\pm^2 \approx y_\pm U - 1 \pm \left[1 + (1+\eta)\left(1 \mp \sqrt{\frac{\eta}{1+\eta}}\right)^2\right]\sqrt{\frac{\eta}{1+\eta}}. \tag{10}$$

https://doi.org/10.1017/S0022377800008436 Published online by Cambridge University Press

Equation (10) yields

$$y_{\pm} \approx \frac{U}{2}\left\{1+\sqrt{1-\frac{4}{U^2}\pm\frac{4}{U^2}\left[1+(1+\eta)\left(1\mp\sqrt{\frac{\eta}{1+\eta}}\right)^2\right]\sqrt{\frac{\eta}{1+\eta}}}\right\}. \tag{11}$$

Assuming U large enough, the square root can be expanded around 1. Upon substraction of $y_+ - y_-$, we obtain to leading order

$$\Delta y = y_+ - y_- \approx \frac{4\sqrt{\eta(1+\eta)}}{U}. \tag{12}$$

This relation shows that the unstable range of the spectrum becomes narrower and narrower as U increases. This effect can be clearly seen on comparing Fig. 3(b) with 3(c).

Thus, whenever $x \gg 1$, the growth rate is given by (4) and the instability is beam-resonant.

This instability has been called the electron/ion whistler instability by Akimoto et al. (1987), who have also calculated the maximum growth rate:

$$\frac{\gamma}{\Omega_p} \approx 0.76\frac{\eta}{1+\eta}, \tag{13}$$

This result was obtained on the basis of the assumption that $\xi_b = |\omega - yV_b + \Omega_p)|/\sqrt{2}\,kv_{\mathrm{the}} \ll 1$, where $v_{\mathrm{the}} = (KT/M)^{1/2}$. However, the maximum growth rate occurs for $\xi_b = 0.7$, which is not much smaller than one. Moreover, one would expect the maximum growth rate to be temperature-dependent.

The growth rates for other instability regions can also be calculated from (3). Since the unstable regions are the result of the merging of the ion-beam branch of the dispersion relation with the electron–magnetosonic branch, one would expect that all right-hand instabilities are beam-resonant.

Thus, assuming $x > 1 \gg |x - yU + 1|$, from (3), we obtain,

$$\Gamma^2 \approx -\frac{(1+x-yU)^2}{1+\eta} + \frac{\eta}{(1+\eta)\,[1-1/(1+x)^2]}. \tag{14}$$

It follows from this equation that, to the extent that the last factor can be neglected with respect to 1, the instability satisfying these conditions is also beam-resonant and the maximum is given by (5).

Finally, assuming $1 \gg (1+x-yU)^2 \gg x$, which is the instability region for low-frequency right-hand waves when $U \gg 1$ (see Fig. 2e), (3) can be approximated by

$$\Gamma^4 + (x - yU + 1)^2\Gamma^2 - \frac{\eta}{1+\eta} \approx 0. \tag{15}$$

Therefore

$$\Gamma^2 \approx -\frac{1}{2}(1+x-yU)^2 + \sqrt{\frac{1}{4}(1+x-yU)^4 + \frac{\eta}{1+\eta}}. \tag{16}$$

In this case too, the maximum growth rate occurs for $x - yU \approx -1$, i.e., this is also a beam-resonant instability. The maximum growth rate is given by

$$\Gamma \simeq \left(\frac{\eta}{1+\eta}\right)^{1/4}, \tag{17}$$

https://doi.org/10.1017/S0022377800008436 Published online by Cambridge University Press

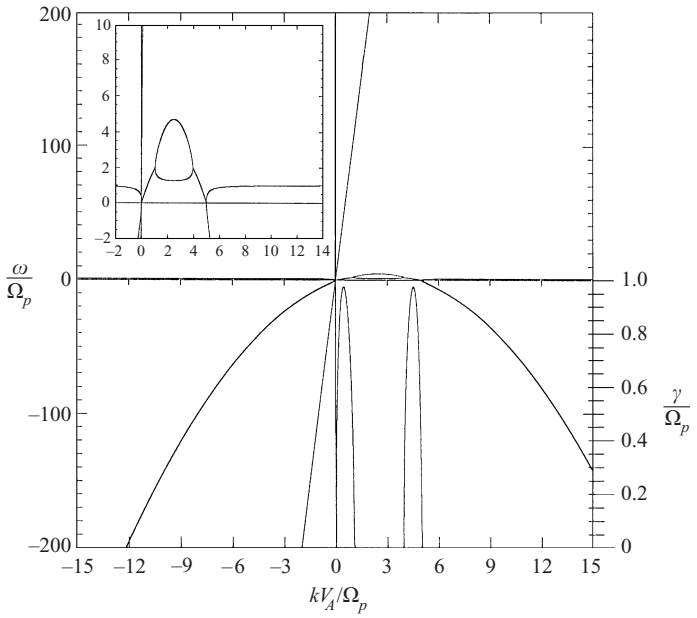

Figure 4. As Fig. 2, but for $\eta = 0.05$ and $U = 100$.

and the instability range behaves like $1/U_b$.

Thus all right-hand polarized instabilities are beam-resonant.

For left-hand polarized waves, assuming that $yU \gg 1-x$, and also that $yU \gg \Gamma$, it follows from (3) that

$$\Gamma^2 y^2 U^2 + (1-x)^2 y^2 U^2 - \frac{y^2 U^2}{1+\eta} \approx 0. \tag{18}$$

Thus

$$\Gamma^2 \approx \frac{1}{1+\eta} - (1-x)^2. \tag{19}$$

It follows from (19) that the maximum growth rate occurs at $1-x \approx 0$, and is given by

$$\Gamma \approx \sqrt{\frac{1}{1+\eta}}. \tag{20}$$

It can also be shown that for $U \geqslant 1$, the instability range is proportional to $1/U$, so that this instability becomes narrower as U increases.

According to this result, for $\eta \ll 1$, the maximum growth becomes of order one independently of the actual value of 2. It should be noted that as η becomes smaller and smaller, a larger and larger beam velocity is required to trigger the higher-frequency branch of the left-hand instability. Note that already for $\eta = 0.4$, a beam velocity of $U \approx 11.4$ is required in order to destabilize the higher-frequency branch (see Fig. 1). It follows from a numerical analysis of (2) that the maximum growth rates of both left-hand instabilities are indeed of order one, as illustrated in Fig. 4 for $\eta = 0.05$ and $U = 100$. We want to emphasize the fact that, for such small beam concentrations, the higher-frequency branch of the spectrum becomes unstable only for very large beam velocities. For

https://doi.org/10.1017/S0022377800008436 Published online by Cambridge University Press

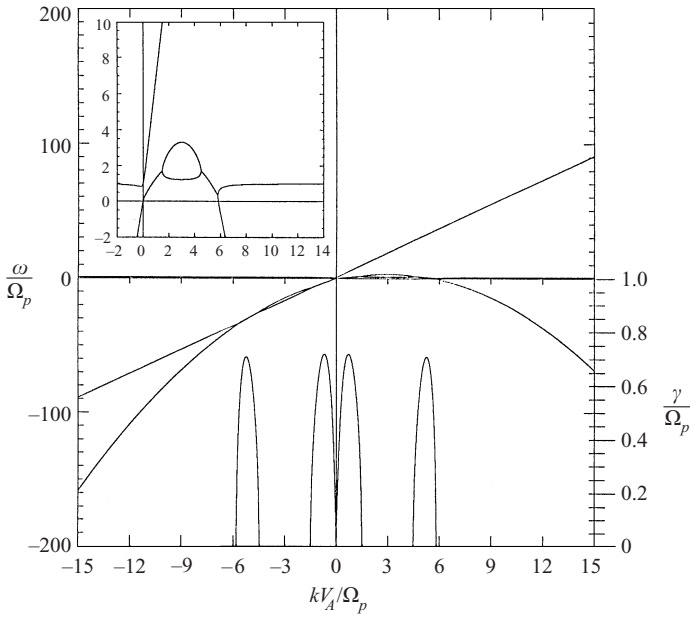

Figure 5. As Fig. 2, but for $\eta = 1$ and $U = 6$.

example, for $\eta = 0.1$, the threshold beam velocity is $U \approx 42$, and it gets larger and larger for decreasing beam concentration.

It follows from (5) and (14) that whenever the four instabilities are present, their maximum growth rates are the same when $\eta = 1$. This result, which also follows from symmetry considerations, is illustrated in Fig. 5 for $\eta = 1$ and $U = 6$.

3. Thermal effects

In Gomberoff and Astudillo (1998), it was shown that, in general, thermal effects reduce the growth rates of the cold-plasma instabilities, and lead to a broadening of the instability range. However, in the case of the electron/ion whistler instability, a thermal anisotropy in the ion beam leads to an increase in the corresponding growth rate (Wong and Goldstein 1986).

To illustrate this effect, we solve (1) numerically for right-hand polarized waves. In order to obtain the dispersion relation for right-hand polarized waves, one has to change in (1), x and y to -x and -y. Thus, in Fig. 6, we have taken for the core and beam temperatures $\beta_c = 1$ and $\beta_b = 1$, for $\eta = 0.1$ and $U = 12$. The corresponding dispersion relation for right-hand waves and growth rates are shown. Growth rates for the cold-plasma case are shown by crosses, and those for the thermal effects by full lines. It follows from Fig. 6(a) that the high-frequency unstable region is affected by thermal effects, leading to a reduction in the growth rate and a broadening of the spectrum. In contrast, the growth rate of the low-frequency part of the unstable spectrum is decreased, but the unstable range is not affected in any appreciable way.

In Fig. 6(b), we have considered the effect of thermal anisotropy in the beam distribution function. As follows from the figure, a thermal anisotropy of $A_b = 5$ leads to an increase in the growth rate of the high-frequency unstable region.

https://doi.org/10.1017/S0022377800008436 Published online by Cambridge University Press

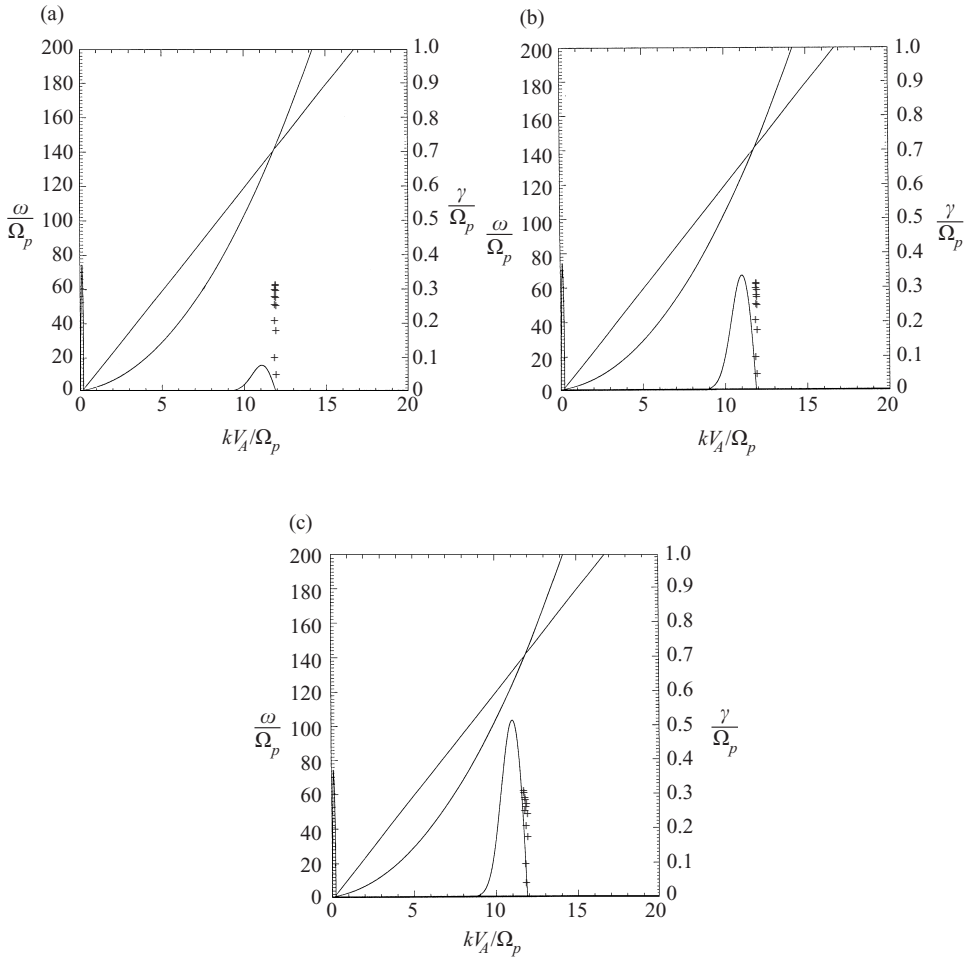

Figure 6. (a) Dispersion relation, x versus y, for right-hand waves for the parameters $\beta_c = 1$, $\beta_b = 1$, $\eta = 0.1$, $U_b = 12$, $A_c = 1$, and $A_b = 1$. The curves at the bottom of the figure are the corresponding growth rates. The lines with crosses correspond to the growth rates of the cold-plasma case, and the full lines to the growth rates of the hot case. (b) As (a), but for $A_b = 5$. (c) As (a), but for $A_{\rm b} = 8$.

Finally, in Fig. 6(c), we have increased A_b to $A_b = 8$ in order to show that the effect can be very important for large beam thermal anisotropies. The growth rate is greatly increased and the instability range is enhanced. The low-frequency branch remains unchanged.

4. Summary

We have shown that an ion beam can lead to four types of electromagnetic instabilities. In the frame where the ion core is at rest, these correspond to two right-hand and two left-hand polarized instabilities, leading to electromagnetic waves propagating in the direction of the external magnetic field. All of these instabilities are present in a cold plasma.

For any given beam concentration and sufficiently large ion-beam velocity, there are always two right-hand and two left-hand polarized instability regions.

https://doi.org/10.1017/S0022377800008436 Published online by Cambridge University Press

All right-hand instabilities are beam-resonant, satisfying $\omega - yV_b + \Omega_p \approx 0$ around their maximum growth rate. The two left-hand polarized instabilities are ion-cyclotron resonant, satisfying $\omega \approx \Omega_p$ around the maximum. The right-hand resonant instabilities become more and more monochromatic as U increases. The maximum growth rates depend only on the ratio between the beam density and the total density.

On the other hand, the growth rate of the left-hand polarized waves depends on the ratio between the core density and the total density for sufficiently large beam velocities. This means that, for small η, the growth rate approaches the value 1. This is not a surprising result, since the free-energy source of the instability is the beam velocity, and the beam velocity required to destabilize the higher-frequency branch of the left-hand polarized waves becomes larger and larger as the beam concentration decreases.

In general, thermal effects reduce the growth rate of the cold-plasma instabilities and lead to a broadening of the unstable range. However, a thermal anisotropy in the ion beam can lead to an increase in the growth rate of the electron/ion whistler instability. The low-frequency branch of the right-hand waves is not affected by the thermal anisotropy. The growth rate of this branch is reduced by thermal effects, but the instability range remains unchanged. In contrast, the instability range of the high-frequency branch is largely enhanced owing to thermal effects.

Acknowledgements

This work has been partially supported by FONDECYT Grants 1990047 and 1971324, and Fundación Andes Grant C-12999/6.

References

Akimoto, K. and Winske, D. 1989 Nonlinear generation of whistler waves by an ion beam. *J. Geophys. Res.* **94**, 17259.

Akimoto, K., Gary, S. P. and Omidi, M. 1987 Electron/ion whistler instabilities and magnetic noise bursts. *J. Geophys. Res.* **92**, 11209.

Akimoto, K., Winske, D., Gary, S. P. and Thomsen, M. F. 1993 Nonlinear evolution of electromagnetic ion beam instabilities. *J. Geophys. Res.* **98**, 1419.

Brinca, A. L. and Tsurutani, B. T. 1988a Survey of low-frequency electromagnetic waves simulated by two coexisting newborn ion species. *J. Geophys. Res.* **93**, 48.

Brinca, A. L. and Tsurutani, B. T. 1988b Temperature effects on the pickup process of water group and hydrogen ions: extension of 'A theory for low-frequency waves observed at comet Giacobinni–Zinner'. *J. Geophys. Res.* **93**, 243.

Brinca, A. L., Sckopke, N. and Pashmann, G. 1990 Wave excitation downstream of the low-β, quasi-perpendicular bow shock. *J. Geophys. Res.* **95**, 6331.

Coates, A. J., Johnstone, A. D., Huddleston, D. E., Wilken, B., Jockers, K. and Glassmeir, K. H. 1989 Velocity space diffusion of pick-up ions from the water group at comet Halley. *J. Geophys. Res.* **94**, 9983.

DeCoster, R. J. and Frank, L. A. 1979 Observations pertaining to the dynamics of the plasma sheet boundary layer. *J. Geophys. Res.* **84**, 1553.

Eastman, T. E., Frank, L. A., Peterson, W. K. and Lennardson, W. 1984 The plasma sheet boundary layer. *J. Geophys. Res.* **89**, 1553.

Feldman, W. C., Asbridge, J. R. and Bame, S. J. 1974 Bow shock perturbation of the upstream solar wind proton component. *J. Geophys. Res.* **79**, 2773.

Forbes, T. G., Hones, E. W., Bame, S. J., Asbridge, J. R., Pashmann, G., Skopke, N. S. and Russell, C. T. 1981 Evidence for the tailward retreat of a magnetic neutral line in the magnetotail during substorm recovery. *Geophys. Res. Lett.* **8**, 261.

Fried, B. D. and Conte, S. D. 1961 *The Plasma Dispersion Function*. Academic Press, San Diego.

Gary, S. P. 1991 Electromagnetic ion/ion instabilities and their consequences in space plasmas: a review. *Space Sci. Rev.* **56**, 373.

Gnavi, G., Gomberoff, L., Gratton, F. T. and Galvão, R. M. O. 1996 Electromagnetic ion-beam instabilities in a cold plasma. *J. Plasma Phys.* **55**, 77.

Goldstein, M. and Wong, H. K. 1987 A theory for low-frequency waves observed at comet Giacobinni–Zinner. *J. Geophys. Res.* **92**, 4695.

Gomberoff, L. 1992 Electrostatic waves in the Earth's magnetotail and in comets, and electromagnetic instabilities in the magnetosphere and the solar wind. *IEEE Trans. Plasma Sci.* **20**, 843.

Gomberoff, L. 1995 Circularly polarized Alfvén waves and ion cyclotron waves in space plasmas. *Physica Scripta* **T60**, 144.

Gomberoff, L. and Astudillo, H. F. 1998 Electromagnetic ion-beam–plasma instabilities. *Planet. Space Sci.* **46**, 1683.

Gomberoff, L., Gratton, F. T. and Gnavi, G. 1994 Excitation and parametric decay of electromagnetic ion cyclotron waves in high speed solar wind streams. *J. Geophys. Res.* **99**, 14717.

Gomberoff, L., Gnavi, G. and Gratton, F. T. 1996 Minor heavy ion electromagnetic beam–plasma interactions in the solar wind. *J. Geophys. Res.* **101**, 13517.

Hollweg, J. V., Esser, R. and Jayanti, V. 1993 Modulation and decay instabilities of Alfvén waves: effect of streaming He^{++} ions. *J. Geophys. Res.* **98**, 34991.

Hoppe, M. M., Russell, C. T., Frank, L. A., Eastman, T. E. and Greestadt, E. W. 1981 Upstream hydromagnetic waves and their association with backstreaming ion populations: ISEE 1 and 2 observations. *J. Geophys. Res.* **86**, 4471.

Hoppe, M. N., Russell, C. T., Eastman, T. E. and Frank, L. A. 1982 Characteristics of ULF waves associated with upstream ion beams. *J. Geophys. Res.* **87**, 643.

Neugebauer, M., Lazarus, A. J., Balsiger, M., Fuselier, S. A., Neubauer, F. M. and Rosenbauer, H. 1989 The velocity distribution of cometary protons picked up by the solar wind. *J. Geophys. Res.* **94**, 5227.

Takahashi, K. and Hones, E. W. Jr 1988 ISEE 1 and 2 observations of ion distributions at the plasma sheet–tail lobe boundary. *J. Geophys. Res.* **93**, 8558.

Tsurutani, B. T. and Smith, E. J. 1986 Strong hydromagnetic turbulence associated with comet Giacobinni–Zinner. *Geophys. Res. Lett.* **13**, 258.

Wong, H. K. and Goldstein, M. L. 1987 Proton beam generation of whistler waves in the Earth's bow shock. *J. Geophys. Res.* **92**, 12419.

Wu, S. and Davidson, R. C. 1972 Electromagnetic instabilities produced by neutral-particle ionization in planetary space. *J. Geophys. Res.* **77**, 5399.